JACS
JOURNAL OF THE AMERICAN CHEMICAL SOCIETY
pubs.acs.org/JACS
Article

Conjugation-Modulated Excitonic Coupling Brightens Multiple Triplet Excited States

Tao Wang, Abhishek Kumar Gupta, Sen Wu, Alexandra M. Z. Slawin, and Eli Zysman-Colman*

Cite This: https://doi.org/10.1021/jacs.2c12320
Read Online
ACCESS | Metrics & More | Article Recommendations | Supporting Information

ABSTRACT: The design and regulation of multiple room-temperature phosphorescence (RTP) processes are formidably challenging due to the restrictions imposed by Kasha's rule. Here, we report a general design principle for materials that show multiple RTP processes, which is informed by our study of four compounds where there is modulation of the linker hybridization between donor (D) and acceptor (A) groups. Theoretical modeling and photophysical experiments demonstrate that multiple RTP processes can be achieved in sp^3 C-linked D−A compounds due to the arrest of intramolecular electronic communication between two triplet states (T_1^H and T_1^L) localized on the donor and acceptor or between two triplet states, one localized on the donor and one delocalized across aggregated acceptors. However, for the sp^2 C-linked D−A counterparts, RTP from one locally excited T_1 state is observed because of enhanced excitonic coupling between the two triplet states of molecular subunits. Single-crystal and reduced density gradient analyses reveal the influence of molecular packing on the coincident phosphorescence processes and the origin of the observed aggregate phosphorescence. These findings provide insights into higher-lying triplet excited-state dynamics and into a fundamental design principle for designing compounds that show multiple RTP.

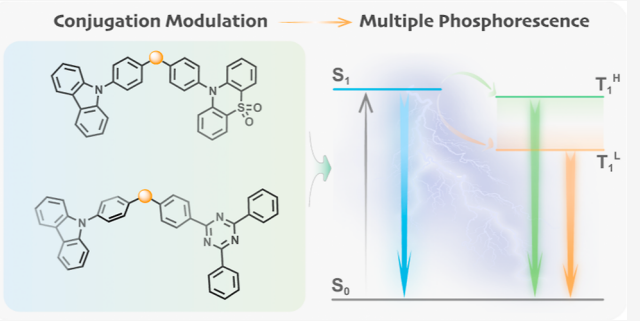

INTRODUCTION

The efficient generation, controllable management, and on-demand migration of triplet excitons from higher-lying to lower-lying triplet excited states in organic molecules have combined to constitute the long-sought Holy Grail of room-temperature phosphorescence (RTP). However, the exciton spin-flip between well-separated singlet and triplet excited states is not allowed due to the violation of Winger's rule.[1,2] To tackle this apparent contradiction, ever-increasingly complex molecular design principles have been devised to modulate both the molecular structure and host−guest interactions.[3−5] Behind these is the control of the relative kinetics of facilitating intersystem crossing (ISC)[6,7] and suppressing nonradiative processes,[8−10] both of which are paramount to achieving efficient RTP. From the perspective of molecular design, introducing heteroatoms, such as N,[11,12] O,[13,14] P,[15−17] and S,[18−20] into metal/halogen-free aromatic compounds is a popular way to enhance the ISC efficiency through the introduction of $n-\pi^*$ states that allow for the spin-flip process to occur, following El-Sayed's rule.[21] Most recently, Marder and co-workers demonstrated that a $(\sigma, B_p) \rightarrow (\pi, B_p)$ transition localized on a three-coordinate boron atom could also accelerate ISC.[22] This new approach likewise relies on El-Sayed's rule to mediate state mixing and thus ISC from S_1 to T_1. To sufficiently brighten the populated triplet excitons of organic compounds, it is also necessary to weaken nonradiative energy dissipation. To date, a plethora of methods, such as engineering molecular crystals,[11,14,23−25] employing a polymer matrix,[26−30] and constructing a rigid host environment,[31−34] have been exploited to achieve suppressed nonradiative decay. Following these principles, many RTP luminophores have been developed, showing moderate photoluminescence (PL) quantum yield (Φ_{PL}) and/or long phosphorescence lifetime (τ_{Ph}). These compounds have been exploited in diverse applications, such as imaging,[35−37] optoelectronics,[38−40] nonlinear optics,[41] and information encryption.[16,18,28,42]

Multiple phosphorescence from a single component is an emergent phenomenon from the radiative decay of excitons from multiple accessible triplet excited states. Compounds that show multiple phosphorescence offer a handle into the study of triplet exciton dynamics. Due to Kasha's rule,[43] it remains a formidable challenge to enable multiple phosphorescence at room temperature, though there are well-studied systems that show anti-Kasha's fluorescence.[44,45] Thus, there have been only a few reports documenting anti-Kasha RTP in organic compounds.[46−48] For example, Wu and co-workers reported

Received: November 20, 2022

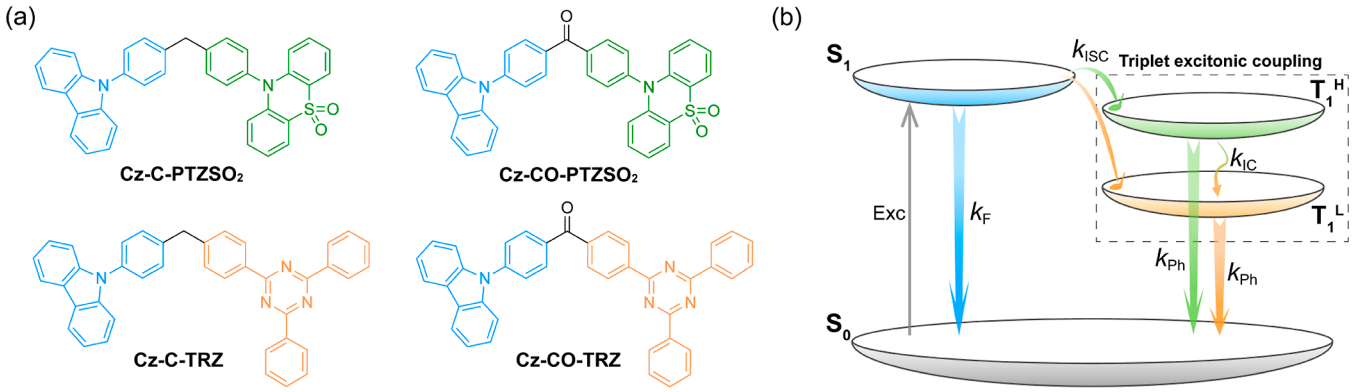

Figure 1. (a) Chemical structures investigated in this study. (b) Schematic illustration of a Jablonski diagram outlining the origin of multiple phosphorescence from T_1^H and T_1^L states. Exc: Excitation; F: fluorescence; Ph: phosphorescence; ISC: intersystem crossing; IC: internal conversion.

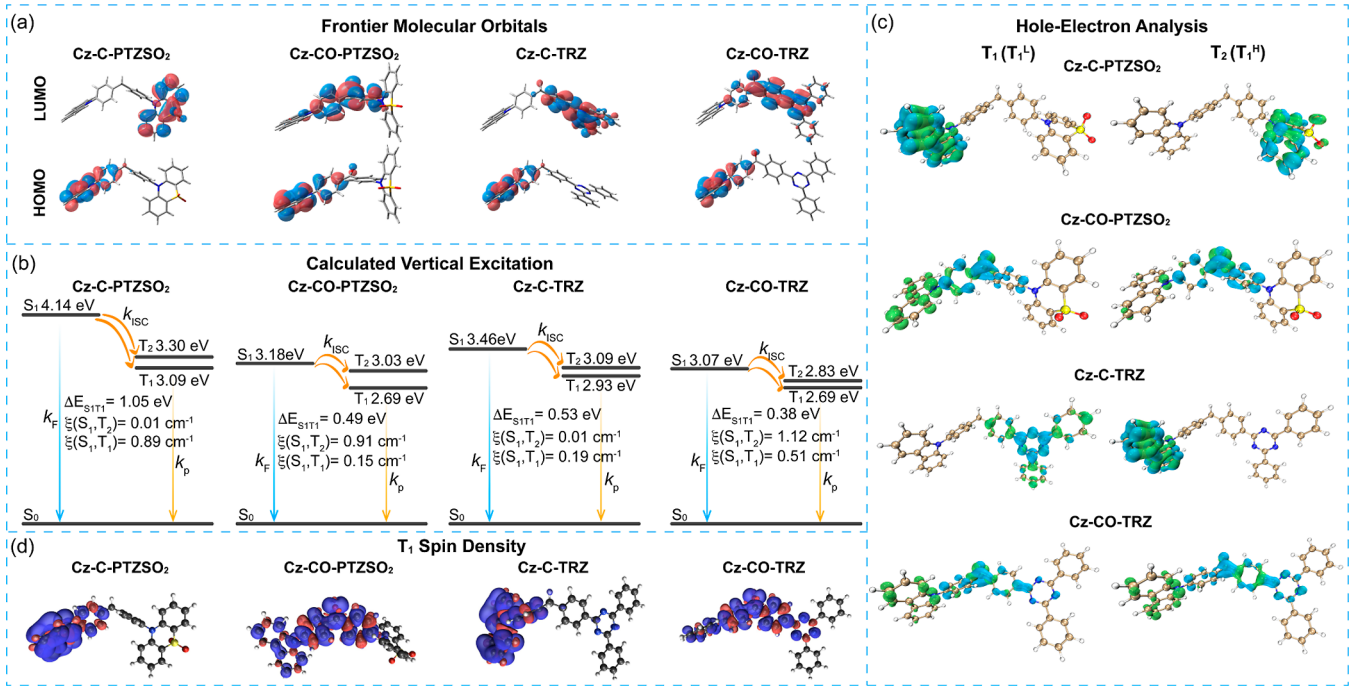

Figure 2. (a) Electron density distribution of the frontier molecular orbitals (isovalue: 0.02) and (b) vertical excitation energy levels of S_1, T_1, and T_2 states calculated at the optimized S_0 geometry in the gas phase at the TD-DFT-PBE0/6-31G(d,p) level; spin−orbit coupling constants calculated at the S_1 geometry. (c) Hole (green)−electron (blue) distribution analysis (isovalue: 0.002) for triplet excited states at the optimized S_0 geometry. (d) T_1 spin density distributions (isovalue: 0.0004) calculated at the optimized T_1 geometry in the gas phase at the uPBE0/6-31G(d,p) level.

that heterocyclic stilbene derivatives exhibited room-temperature dual phosphorescence originating from both T_2 and T_1 states.[47] This results from the relatively large energy gap (>0.5 eV) between these two states, which inhibits the excitonic internal conversion (IC). Room-temperature dual phosphorescence has also been demonstrated in both systems where there is simultaneous emission from monomers and aggregates.[11,49] Recently, T_1 conformer-regulated multiple phosphorescence has been demonstrated by us, which renders the excited-state dynamics tunable via thermal activation.[20,50] However, a general principle to regulate multiple phosphorescence on demand remains elusive.

Here, we present a general multiple RTP design strategy for organic compounds by modulating the excitonic coupling between two T_1 states localized on the donor and acceptor via the degree of conjugation that the linker mediates between these two groups. We define the higher-lying and lower-lying T_1 states as T_1^H and T_1^L states, respectively. By comparing the photophysics of emitters containing sp^3 and sp^2 linkages (C vs CO), we found that dual phosphorescence relies on how strongly the two triplet excited states communicate. It was demonstrated in two examples that sp^3 C-linked compounds (**Cz-C-PTZSO$_2$** and **Cz-C-TRZ**) (Figure 1a), where 9-phenylcarbazole (**Cz-Ph**) serves as the donor and 10-phenyl-10*H*-phenothiazine-5,5-dioxide (**PTZSO$_2$**) or 2,4,6-triphenyl-1,3,5-triazine (**TRZ**) acts as the acceptor (Scheme S1a), could enable dual phosphorescence from two locally excited (^{3}LE) triplet states due to negligible excitonic coupling between donor and acceptor moieties at room temperature (Figure 1b). In contrast, the sp^2 C-linked counterpart (**Cz-CO-PTZSO$_2$**) shows only one ^{3}LE emission at room temperature, together with aggregate phosphorescence in the crystal state, while no RTP was recorded in the other sp^2 C-linked compound (**Cz-CO-TRZ**).

https://doi.org/10.1021/jacs.2c12320
J. Am. Chem. Soc. XXXX, XXX, XXX−XXX

RESULTS AND DISCUSSION

The synthesis of **Cz-C-PTZSO$_2$**, **Cz-CO-PTZSO$_2$**, **Cz-C-TRZ**, and **Cz-CO-TRZ** is outlined in Scheme S1. All samples were purified by repeated silica column chromatography, followed by temperature-gradient vacuum sublimation and finally recrystallization from toluene. The molecular structures and purity were validated by a combination of ^{1}H and ^{13}C nuclear magnetic resonance (NMR) spectroscopy, high-resolution mass spectrometry (HRMS), melting point determination, elemental analysis (EA), and high-performance liquid chromatography (HPLC) (Figures S1−S32).

We hypothesized that the IC between donor- and acceptor-localized T_1 states could be slowed or even inhibited through the use of a nonconjugated sp^3 carbon atom to electronically isolate donor and acceptor groups (**Cz-C-PTZSO$_2$** and **Cz-C-TRZ**), where multiple RTP would originate from both donor and acceptor subunits (Figure 1b). For sp^2 C-linked species (**Cz-CO-PTZSO$_2$** and **Cz-CO-TRZ**), due to the stronger electronic communication between the donor and acceptor, the IC of excitons between the two low-lying triplet states is greatly enhanced, resulting in only phosphorescence from the T_1^L state.

To substantiate this hypothesis, we first modeled the photophysical properties of these four compounds in the gas phase using density functional theory (DFT) at the PBE0[51]/6-31G(d,p) level.[52] From Figure 2a, the highest occupied molecular orbital (HOMO) and lowest unoccupied molecular orbital (LUMO) of **Cz-C-PTZSO$_2$** and **Cz-C-TRZ** are localized on the donor (**Cz-Ph**) and acceptors (**PTZSO$_2$** and **TRZ**), showing a near-zero frontier molecular orbital (FMO) overlap. For **Cz-CO-PTZSO$_2$** and **Cz-CO-TRZ**, the LUMO is delocalized across both the acceptor and the benzophenone core, resulting in deeper HOMO and LUMO levels (Figure S33). Time-dependent DFT calculations at the same level of theory demonstrate a relatively large energy gap between S_1 and T_1 states (ΔE_{ST}) in these compounds (Figure 2b), indicating that these compounds should not exhibit thermally activated delayed fluorescence. Given the presence of multiple triplet state energy levels serving as upper receiver states and moderate spin−orbital coupling constants (Figure S34), RTP should be theoretically favored as the dominant radiative decay process. The T_1 and T_2 energies of **Cz-C-PTZSO$_2$** and **Cz-C-TRZ** are almost degenerated with those of the T_1 energies of the isolated donor, **Cz-Ph**, and acceptors, **PTZSO$_2$** and **TRZ** (Figure S35b). For **Cz-CO-PTZSO$_2$** and **Cz-CO-TRZ**, similar T_1 energies imply that both states have the same character, which is close to that of the LE T_1 state of the carbazole-benzophenone (**Cz-BP**) subunit (Figure S35b). Furthermore, the excitonic coupling between T_1 and T_2 was investigated based on the hole−electron distribution analysis using the Multiwfn program.[53] **Cz-C-PTZSO$_2$** and **Cz-C-TRZ** both show decoupled T_1 and T_2 states (Figure 2c), where the hole (green) and electron (blue) distributions are identical to those of the donor (as the T_1 state for **Cz-C-PTZSO$_2$**; as the T_2 state for **Cz-C-TRZ**) and the acceptor (as the T_2 state for **Cz-C-PTZSO$_2$**; as the T_1 state for **Cz-C-TRZ**) (Figure S35c). Considering that the T_1 and T_2 states are localized on the donor and acceptor subunits and possess almost identical triplet energies with the T_1 energies of the isolated subunits, here we redefine the T_2 and T_1 states as T_1^H and T_1^L states, respectively. According to Fermi's golden rule,[54] the reduced vibronic coupling between T_1^H and T_1^L states should also favor a slow IC, enabling emission from both the donor and acceptor groups. However, **Cz-CO-PTZSO$_2$** and **Cz-CO-TRZ** exhibit strongly coupled triplet excited states due to the overlap of the hole and electron densities as well as the small energy gap between T_1^H and T_1^L states; thus, there should be rapid IC between T_1^H and T_1^L states. T_1 spin density distributions reveal that in **Cz-C-PTZSO$_2$** and **Cz-C-TRZ**, they are localized on **Cz-Ph** (Figure 2d), while for **Cz-CO-PTZSO$_2$** and **Cz-CO-TRZ**, the spin densities are relatively delocalized (Figure 2d), similar to the hole−electron density distribution analysis (Figure 2c). Calculated T_1 energies at the optimized T_1 geometry are 2.86, 2.03, 2.86, and 1.98 eV for **Cz-C-PTZSO$_2$**, **Cz-CO-PTZSO$_2$**, **Cz-C-TRZ**, and **Cz-CO-TRZ**, respectively.

The energies of FMOs were inferred from the oxidation and reduction potentials (E^{ox}/E^{red}), obtained using cyclic voltammetry and differential pulse voltammetry (DPV) in deaerated DMF with 0.1 M [^{n}Bu$_4$N]PF$_6$ as the supporting electrolyte. The E^{ox}/E^{red} values of **Cz-C-PTZSO$_2$**, **Cz-CO-PTZSO$_2$**, **Cz-C-TRZ**, and **Cz-CO-TRZ**, determined from the DPV peaks, are 1.31/−2.32 V, 1.42/−1.52 V, 1.23/−1.73 V, and 1.41/−1.18 V, respectively, versus SCE (Figure 3, Table S1). The corresponding HOMO/LUMO values are −5.66/−2.03, −5.77/−2.83, −5.57/−2.62, and −5.76/−3.17 eV,[55] respectively. The more stabilized HOMO values of **Cz-CO-PTZSO$_2$** and **Cz-CO-TRZ** compared with those of **Cz-C-PTZSO$_2$** and **Cz-C-TRZ** are the result of the presence of the electron-withdrawing benzophenone fragment that stabilizes the HOMO. Very similar HOMO values were calculated for **Cz-C-PTZSO$_2$** and **Cz-C-TRZ**, reflecting the electronically isolated donor in both these compounds (Figure 2a), which is absent in **Cz-CO-PTZSO$_2$** and **Cz-CO-TRZ**. The trends in measured HOMO/LUMO levels coincide with those modeled using DFT (Figure S33).

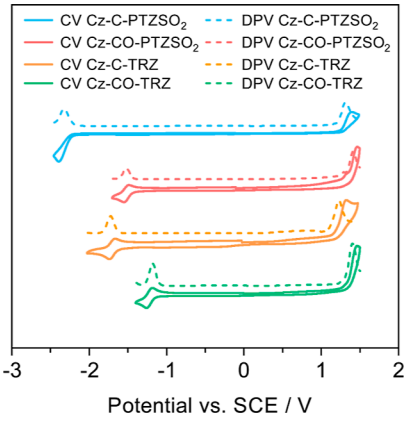

Figure 3. Cyclic voltammogram and differential pulse voltammogram in degassed DMF with 0.1 M [^{n}Bu$_4$N]PF$_6$ as the supporting electrolyte and Fc/Fc$^+$ as the internal reference (0.45 V vs SCE).[55] $E_{HOMO/LUMO} = -(E^{ox}/E^{red} + 4.8)$ eV using values vs Fc/Fc$^+$.[56]

We next investigated the photophysical properties of the **Cz-C-PTZSO$_2$** and **Cz-CO-PTZSO$_2$** crystals, which were isolated from a toluene solution. The photophysical data are summarized in Table S2. The steady-state PL spectrum of **Cz-C-PTZSO$_2$** in air at 298 K shows a structured LE emission profile with peak maxima, λ_{PL}, at 403 and 426 nm, alongside a broad emission tail (Figure 4a). The corresponding PL lifetime, τ_{PL}, is ∼3.5 ns, recorded at both 403 and 426 nm (Figure S36a). When placed under vacuum, the broad PL band was enhanced with λ_{PL} at 403 and 426 nm, indicating the most likely involvement of triplet excited states. Time-gated PL measurements (3 ms delay) detected the RTP spectrum of **Cz-C-PTZSO$_2$**, where dual

https://doi.org/10.1021/jacs.2c12320
J. Am. Chem. Soc. XXXX, XXX, XXX−XXX

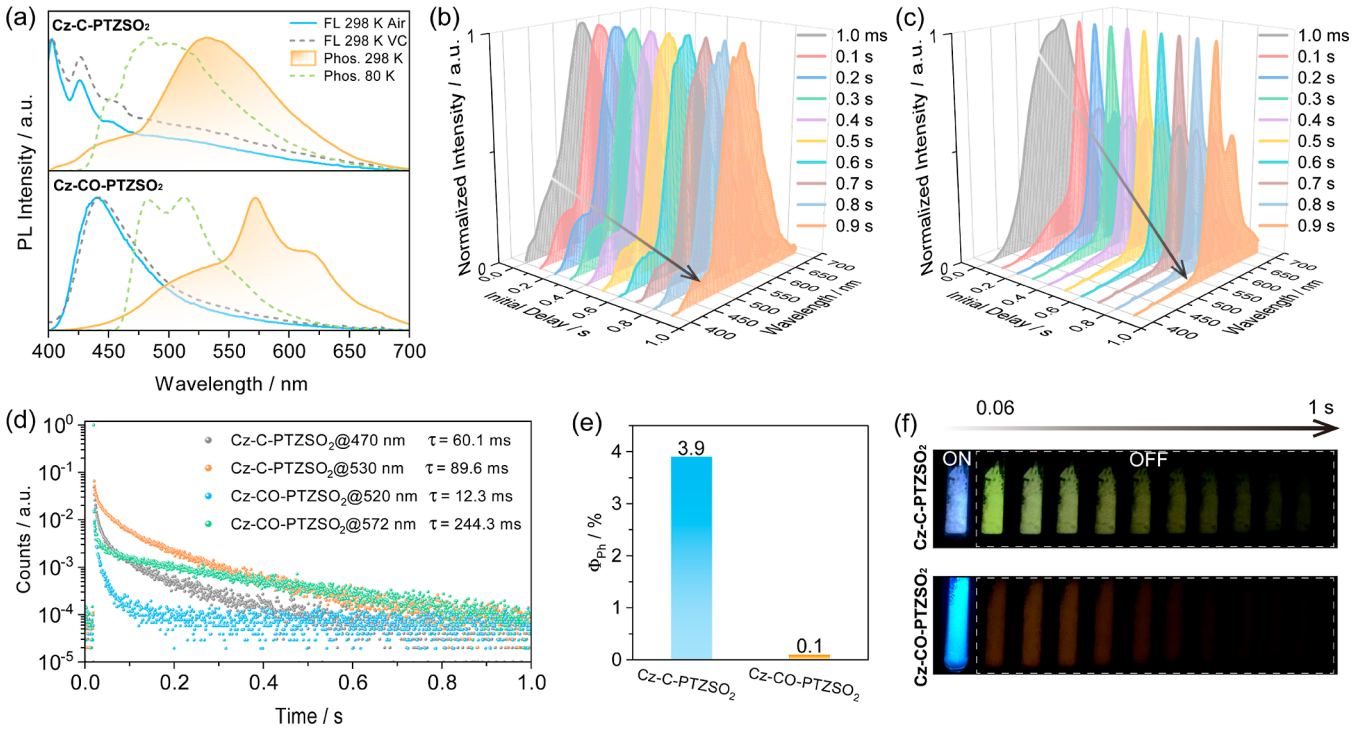

Figure 4. (a) Steady-state PL (in air and in vacuum) and phosphorescence spectra (in vacuum); λ_{exc} = 370 nm; time-gated window: 3 ms to 1 s (**Cz-C-PTZSO$_2$**), 3−200 ms for 298 K and 3 ms to 1 s for 80 K (**Cz-CO-PTZSO$_2$**); VC denotes vacuum. RTP spectra of (b) **Cz-C-PTZSO$_2$** and (c) **Cz-CO-PTZSO$_2$** in vacuum recorded at different delay times and a gate of 100 ms. (d) Time-resolved phosphorescence decay profiles in vacuum at 298 K. (e) RTP Φ_{PL} values in N_2 at 298 K. (f) Images showing phosphorescence afterglow in vacuum at 298 K (excitation source: 365 nm UV torch).

emission bands centered at 470 and 530 nm can be observed (Figure 4a), together with associated average phosphorescence lifetime, τ_{Ph}, values of 60.1 and 89.6 ms (Figure 4d), respectively. Figure 4b shows RTP spectra collected at different delay times, which demonstrate that the RTP at 470 nm decays faster than that at 530 nm, reflecting the results of the RTP lifetime measurements (Figure 4d). These dual emission bands match well with the enhanced LE emission and the emission tail presented in the steady-state PL spectra in vacuum. The phosphorescence spectrum recorded at 80 K blue-shifts to 475 nm and is dominated by a structured blue emission band, whose low-temperature phosphorescence (LTP) lifetime is prolonged to 836.7 ms and longer than that recorded at 530 nm (τ_{Ph} = 536.6 ms) (Figure S37a). In line with the proposed multiple phosphorescence model (Figure 1b), we ascribe the dual RTP emission to result from phosphorescence from each of the **Cz-Ph** and **PTZSO$_2$** moieties. To verify these assignments, we measured the phosphorescence spectra of **Cz-Ph** and **PTZSO$_2$** at 77 K (Figures S38 and S39a). It was found that one of the two RTP emission bands of **Cz-C-PTZSO$_2$** matches the phosphorescence of the **Cz-Ph** monomers (Figure S38), while the low-energy RTP band is red-shifted compared to the phosphorescence of **PTZSO$_2$** (Figure S39a); rather, this phosphorescence aligns with the phosphorescence of **PTZSO$_2$** aggregates (Figure S39a). Time-gated phosphorescence measurements of **Cz-C-PTZSO$_2$** recorded in dilute 2-MeTHF glass at 77 K reveal the evolving structured phosphorescence spectra as a function of time (Figure S40a). Distinct from the phosphorescence behavior observed in the crystal, in 2-MeTHF glass, dual phosphorescence is observed originating from LE phosphorescence of the **Cz-Ph** donor (T_1^L) and **PTZSO$_2$** acceptor (T_1^H), which aligns with the DFT calculations.

The behavior of **Cz-CO-PTZSO$_2$** is different. The steady-state PL spectra in air and vacuum at 298 K are similar (λ_{PL} = 440 nm) (Figure 4a), with a PL lifetime of 0.7 ns (Figure S36b). Although dual RTP behavior was recorded, it differs from that of **Cz-C-PTZSO$_2$**. The blue RTP emission band from **Cz-Ph** is absent in **Cz-CO-PTZSO$_2$**, but a new structured RTP emission band is present at λ_{PL} of 572 nm. At 80 K, the phosphorescence emission blue-shifts to the green emission range, whose low-temperature LTP lifetime is 89.8 ms (Figure S37b). We assigned dual phosphorescence to originate from dual emission from the monomer and the aggregates, which is consistent with the recorded PL spectra of the model systems. The computed hole−electron distribution analysis revealed that the phosphorescence of **Cz-CO-PTZSO$_2$** results from LE T_1 emission from **Cz-BP** (Figure 2c). Therefore, we measured the phosphorescence spectrum of **Cz-BP** at 77 K (Figure S39b), which coincides with the green RTP emission band of **Cz-CO-PTZSO$_2$**. We can therefore assign this band to phosphorescence from the **Cz-BP** moiety. To determine the origin of the orange RTP emission, we collected RTP spectra at various delay times. The results revealed that the RTP at 520 nm decays much faster than the RTP at 572 nm (Figure 4c), with corresponding τ_{Ph} of 12.3 ms and 244.3 ms, respectively (Figure 4d). By closer inspection of the phosphorescence spectra of dilute samples in 2-MeTHF glass at 77 K, we found that the emission centered at 572 nm vanished (Figure S41b), implying that the lower-energy RTP of **Cz-CO-PTZSO$_2$** crystals originates from aggregates. As a result, we can conclude that dual phosphorescence of **Cz-CO-PTZSO$_2$** belongs to the mixture of T_1 emission of the monomer and aggregates rather than T_1^H and T_1^L emissions from different subunits. The Φ_{PL} values of **Cz-C-PTZSO$_2$** and **Cz-CO-PTZSO$_2$** at 298 K in air are 5.9 and 4.6%, respectively, which improve to 8.2 and 4.7% under a N_2 atmosphere, respectively

https://doi.org/10.1021/jacs.2c12320
J. Am. Chem. Soc. XXXX, XXX, XXX−XXX

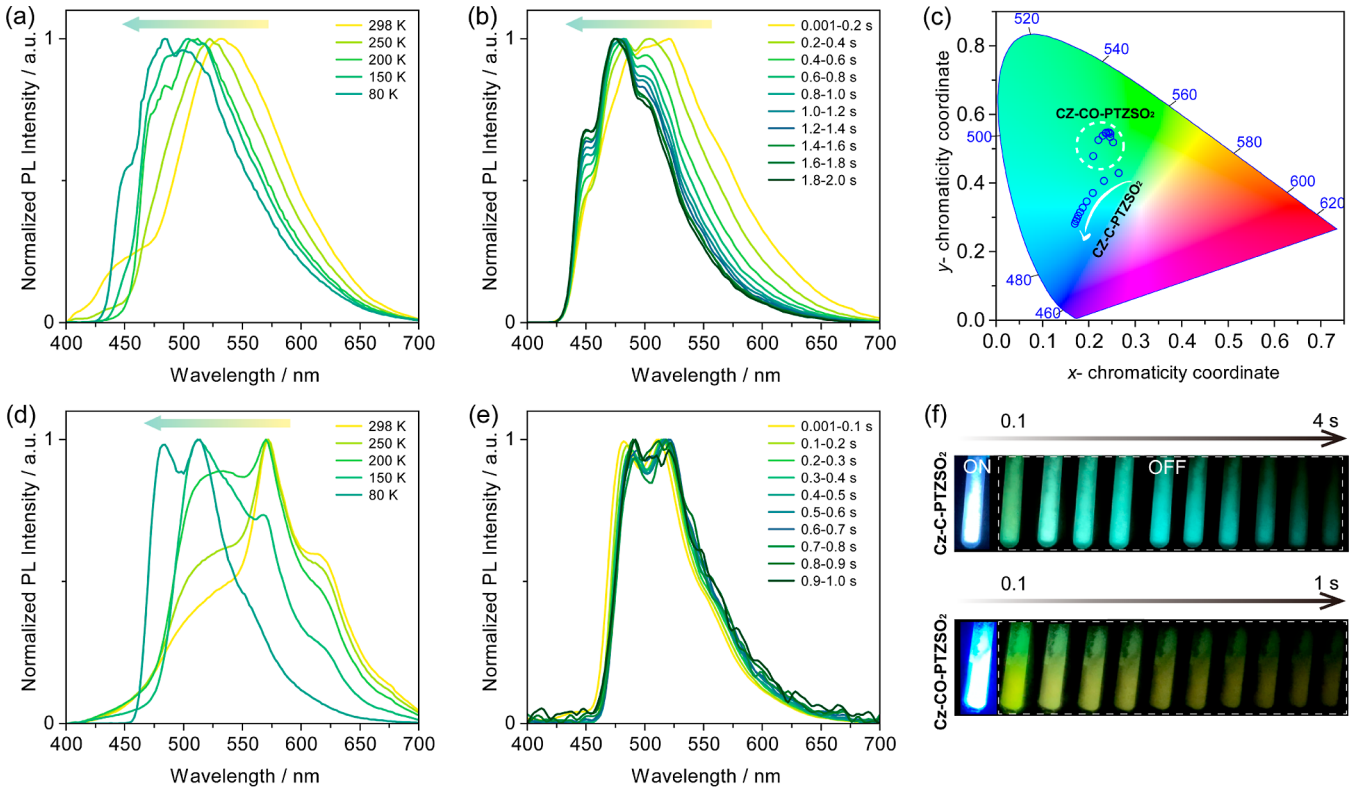

Figure 5. Temperature-dependent phosphorescence spectra of (a) **Cz-C-PTZSO$_2$** (time-gated window: 3 ms to 1 s) and (d) **Cz-CO-PTZSO$_2$** (time-gated window: 3−200 ms for 298−150 K; 3 ms to 1 s for 80 K); λ_{exc} = 370 nm. Phosphorescence of (b) **Cz-C-PTZSO$_2$** and (e) **Cz-CO-PTZSO$_2$** at 80 K recorded at various time-gated windows. (c) CIE coordinates of phosphorescence at 80 K of **Cz-C-PTZSO$_2$** and **Cz-CO-PTZSO$_2$** as a function of time-gated windows shown in (b,e). (f) Images showing phosphorescence afterglows in vacuum at 77 K (excitation source: 365 nm UV torch).

(Table S2). Therefore, the calculated RTP Φ_{PL} values of **Cz-C-PTZSO$_2$** and **Cz-CO-PTZSO$_2$** in N_2 are approximately 4% and 0.1%, respectively (Figure 4e). The weaker RTP of **Cz-CO-PTZSO$_2$** may be caused by the presence of increased nonradiative channels. Figure 4f shows the RTP afterglows of **Cz-C-PTZSO$_2$** and **Cz-CO-PTZSO$_2$** in vacuum.

Further, temperature-dependent PL measurements were conducted to interrogate the origin of the multiple phosphorescence. For **Cz-C-PTZSO$_2$**, the apparent blue shift of the phosphorescence emission occurs as the temperature decreases (Figure 5a), indicating that phosphorescence from **Cz-Ph** gradually dominates the spectral profile at lower temperatures. At 80 K, blue-shifted and structured phosphorescence spectra at different time-gated windows were observed, which confirmed that phosphorescence from T_1^H and T_1^L states of **Cz-C-PTZSO$_2$** is dominated by the LE emission from the **Cz-Ph** and **PTZSO$_2$** groups (Figure 5b), respectively, as these spectra align with those of the phosphorescence spectra of **Cz-Ph** monomers and **PTZSO$_2$** aggregates (Figures S38 and S39a); the T_1^H and T_1^L energies, estimated from the emission peak maxima, are 2.36 and 2.64 eV, respectively. The related Commission Internationale de l'Éclairage (CIE) diagram reflects the gradual emission color change across different time-gated windows (Figure 5c). The images of **Cz-C-PTZSO$_2$** also evidence that the afterglow gradually varies from green to blue (Figure 5f). The approximated calculated slow IC rate between T_1^H and T_1^L indicates that there is weak communication between the two triplet excited states associated with the donor and acceptor subunits (Table S3), which explains the occurrence of T_1^H phosphorescence. A similar scenario was observed in **Cz-CO-PTZSO$_2$**, where temperature-dependent phosphorescence blue-shifts as a function of decreasing temperature (Figure 5d). However, at 80 K, phosphorescence from **Cz-BP** dominates the emission, independent of the time-gated window (Figure 5e). The CIE diagram and images of afterglows document the unchanged phosphorescence color (Figure 5c,f) over time, indicating that the emission results from phosphorescence originating from the **Cz-BP** moiety of **Cz-CO-PTZSO$_2$** (i.e., from the T_1 state). The ΔE_{ST} of **Cz-C-PTZSO$_2$** and **Cz-CO-PTZSO$_2$** in dilute samples in 2-MeTHF glass at 77 K, estimated from the difference in energy between the onsets of the prompt and delayed emission spectra, are 0.28 and 0.41 eV, respectively (Figure S41); it should be noted that ΔE_{ST} of **Cz-C-PTZSO$_2$** is in fact the energy gap between S_1 and T_1^H states (**Cz-Ph**).

Next, the photophysical properties of the **Cz-C-TRZ** and **Cz-CO-TRZ** crystals were investigated. There is no obvious change to the steady-state PL spectra of **Cz-C-TRZ** in air and vacuum, centered at 448 nm (Figure 6a), whose PL lifetime is 5.1 ns measured at 298 K in air (Figure S42a). At 298 K, time-gated PL measurements detected two well-separated phosphorescence bands centered at 460 and 575 nm, with associated lifetimes of 7.1 and 197 ms, respectively (Figure 6b). However, at 80 K, only one green phosphorescence band at 515 nm (τ_{Ph} = 400 ms, Figure S43) was observed (Figure 6a). Compared to the phosphorescence spectra of each of **Cz-Ph** and **TRZ** (Figures S38 and S39c), we conclude that blue RTP and green LTP originate from states localized on **Cz-Ph** and **TRZ**, denoted as T_1^H and T_1^L, respectively, similar to the theoretical prediction (Figure 2c). Similarly, variation of the relative intensity of the structured phosphorescence spectrum of **Cz-C-TRZ** in 2-MeTHF glass recorded at 77 K at different time-gated windows also evidences contributions from the emission from both the

https://doi.org/10.1021/jacs.2c12320
J. Am. Chem. Soc. XXXX, XXX, XXX−XXX

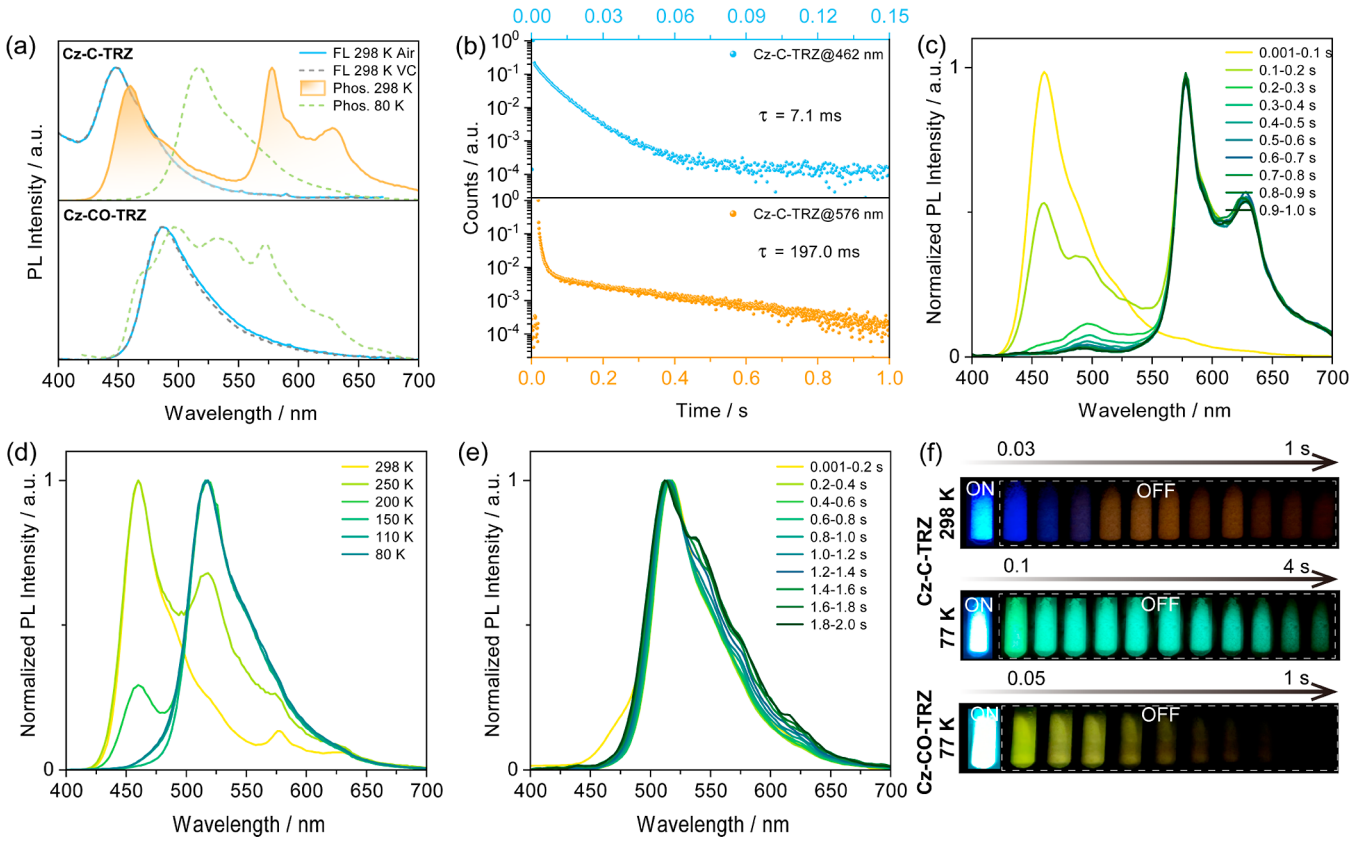

Figure 6. (a) Steady-state PL (in air and in vacuum) and phosphorescence spectra (in vacuum); λ_{exc} = 370 nm; time-gated window: 0.05−1 s for 298 K and 0.05−2 s for 80 K (**Cz-C-TRZ**), 0.05−0.8 s for 80 K for **Cz-CO-TRZ**. (b) Time-resolved phosphorescence decay profiles of **Cz-C-TRZ** in vacuum at 298 K. Phosphorescence spectra of **Cz-C-TRZ** in vacuum at (c) 298 and (e) 80 K recorded at different delay times and a gate of 100 ms. (d) Temperature-dependent phosphorescence spectra of **Cz-C-TRZ**; time-gated window: 3 ms to 1 s. (f) Images showing phosphorescence afterglows in vacuum (excitation source: 365 nm UV torch).

T_1^H and T_1^L states associated with the **Cz-Ph** and **TRZ** moieties, respectively (Figure S40b). Given that the **TRZ** moiety is prone to forming $\pi-\pi$ stacked assemblies, we postulated that the orange RTP likely originates from molecular aggregates. To better elucidate the origin of the multiple triplet excited states, phosphorescence spectra were recorded at different time-gated windows. As shown in Figure 6c, at early time, blue RTP is dominant. Then, emission from aggregates dominates the overall RTP emission, accompanied by a small contribution from the **TRZ** phosphorescence at around 500 nm. The RTP afterglow color of **Cz-C-TRZ** varies from blue to orange (Figure 6f). Temperature-dependent phosphorescence measurements also documented that multiple emissive triplet states exist in the **Cz-C-TRZ** crystals (Figure 6d). At 80 K, LTP emission negligibly changes with time (Figure 6e), reflected by the observed unchanged LTP afterglow (Figure 6f). To further confirm that the orange RTP is from aggregates, the RTP emission of **Cz-C-TRZ** crystals after grinding was recorded. We found that the overall RTP intensity was weakened, where the blue RTP intensity ratio was increased compared to the orange RTP due to the disrupted intermolecular interactions in the aggregates (Figure S44). We prepared **Cz-C-TRZ** crystals via slow sublimation, which we hypothesized would produce samples with increased $\pi-\pi$ stacking. These samples of **Cz-C-TRZ** show stronger orange RTP and negligible blue RTP (Figure S45a,b,e). The RTP lifetime and RTP Φ_{PL} of **Cz-C-TRZ** crystals that were acquired via temperature-gradient vacuum sublimation increase to 540.3 ms and 3.0%, respectively (Figure S46a, Table S4) compared to the respective values of the **Cz-C-TRZ** crystals (τ_{Ph} = 190.7 ms, RTP Φ_{PL} = 0.6%) isolated from toluene. At 80 K, green LTP from **TRZ** centered at 500 nm was also observed, likely due to the suppression of nonradiative processes (Figure S45c), whose lifetime is prolonged to 820.8 ms (Figure S46b). For **Cz-CO-TRZ**, steady-state PL spectra show an unstructured emission centered at 486 nm at room temperature (Figure 6a), whose overall Φ_{PL} and lifetime in air are 13.9% and 2.4 ns, respectively (Table S2, Figure S42b). Unfortunately, no RTP was observed, probably resulting from the strong nonradiative decay. A broad and structured LTP profile was recorded at 80 K (Figure 6a). Time-gated PL measurements reflect that the LTP results from LE emission contributions from each of **Cz-Ph**, **Cz-BP**, and **TRZ** (Figure S47) based on the cross-comparison with the LTP from each of these isolated compounds (Figures S38 and S39b,c). The low-temperature multiple phosphorescence bands may result from restricted molecular conformations that lead to weak electronic coupling at low temperature.[20,57]

We then investigated the single-crystal structures of **Cz-C-PTZSO$_2$**, **Cz-CO-PTZSO$_2$**, and **Cz-C-TRZ** to determine what influence if any intermolecular interactions would have on the observed multiple phosphorescence. For **Cz-C-PTZSO$_2$**, strong CH···O and O···π intermolecular interactions exist between **PTZSO$_2$** moieties (Figure 7a), which is consistent with the assignment that the T_1^L emission of **Cz-C-PTZSO$_2$** at room temperature is almost identical to that from the acceptor **PTZSO$_2$** aggregates. No intermolecular interactions were found

https://doi.org/10.1021/jacs.2c12320
J. Am. Chem. Soc. XXXX, XXX, XXX−XXX

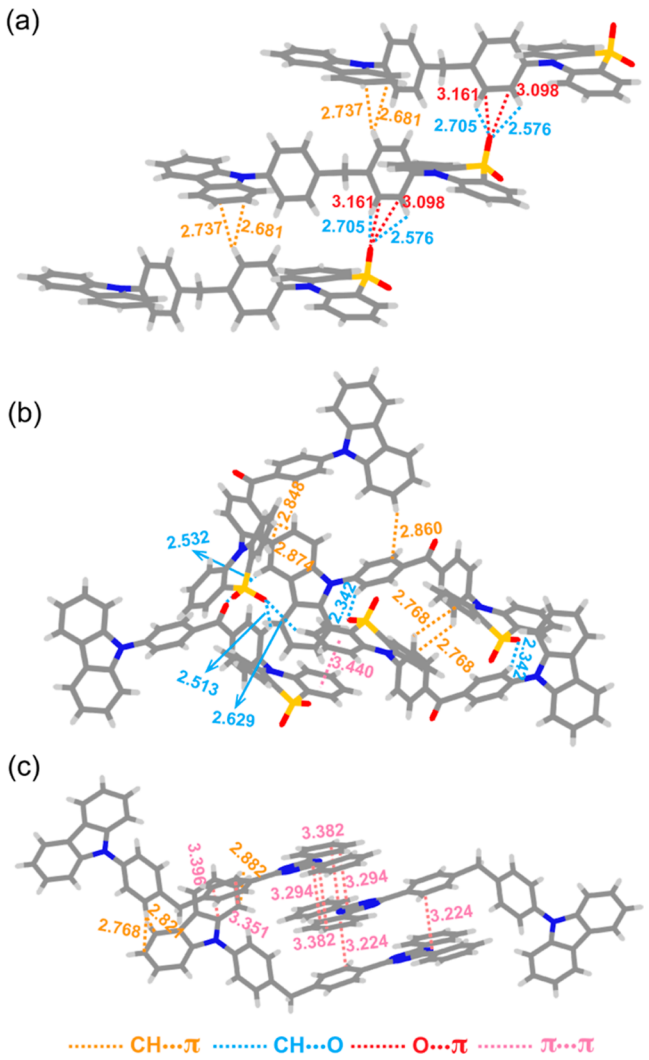

Figure 7. Single-crystal structures of (a) **Cz-C-PTZSO$_2$**, (b) **Cz-CO-PTZSO$_2$**, and (c) **Cz-C-TRZ** showing intermolecular interactions. The distance unit is Å.

between the **Cz-Ph** fragments, implying that the emission from the T_1^H state is from monomeric **Cz-Ph**. For **Cz-CO-PTZSO$_2$**, intermolecular CH···π, CH···O, and π···π interactions are present (Figure 7b), which is consistent with the orange RTP of **Cz-CO-PTZSO$_2$** originating from **Cz-CO-PTZSO$_2$** aggregates, in addition to the green RTP from the **Cz-BP** moiety. For **Cz-C-TRZ**, π···π intermolecular interactions exist between adjacent TRZ fragments (Figure 7c), which result in excitonic splitting and thus a lower T_1 energy (orange RTP). Similar to **Cz-C-PTZSO$_2$**, no apparent intermolecular interactions exist between the adjacent **Cz-Ph** groups, resulting in the occurrence of RTP from **Cz-Ph** in **Cz-C-TRZ**.

In addition, intermolecular interactions were studied in silico by employing noncovalent interaction calculations[58] implemented in the Multiwfn program.[53] The geometries of the emitters are those in the single crystals. As shown in Figure 8a, green spikes of the reduced density gradient (RDG), where the electron density is near zero, confirm the existence of intense van der Waals interactions, which can suppress molecular motions resulting in reduced nonradiative decay in the solid state. The RDG isosurfaces of **Cz-C-PTZSO$_2$** reveal noncovalent interactions between the **PTZSO$_2$** groups (Figure 8b) and negligible interactions between **Cz-Ph** groups, similar to the conclusions drawn from the single-crystal analysis. For **Cz-CO-PTZSO$_2$**, evident noncovalent interactions are distributed across the entirety of the molecules, implicating that the orange RTP belongs to **Cz-CO-PTZSO$_2$** aggregates. As anticipated, π−π interactions are present in the **TRZ** moiety of **Cz-C-TRZ** and CH···π and π···π interactions exist between **Cz-Ph** and **TRZ**. As a result, molecular packing of **Cz-C-TRZ** influences the occurrence of dual RTP, where condensed molecular packing results in strong **Cz-Ph** and **TRZ** interactions and thus efficient triplet−triplet energy transfer (TTET); that is, only orange RTP can be observed in this instance.

CONCLUSIONS

Herein, we have reported a general multiple RTP design principle and validated it using four organic compounds (**Cz-C-PTZSO$_2$**, **Cz-CO-PTZSO$_2$**, **Cz-C-TRZ**, and **Cz-CO-TRZ**). DFT calculations demonstrated that for sp^3 C-linked com-

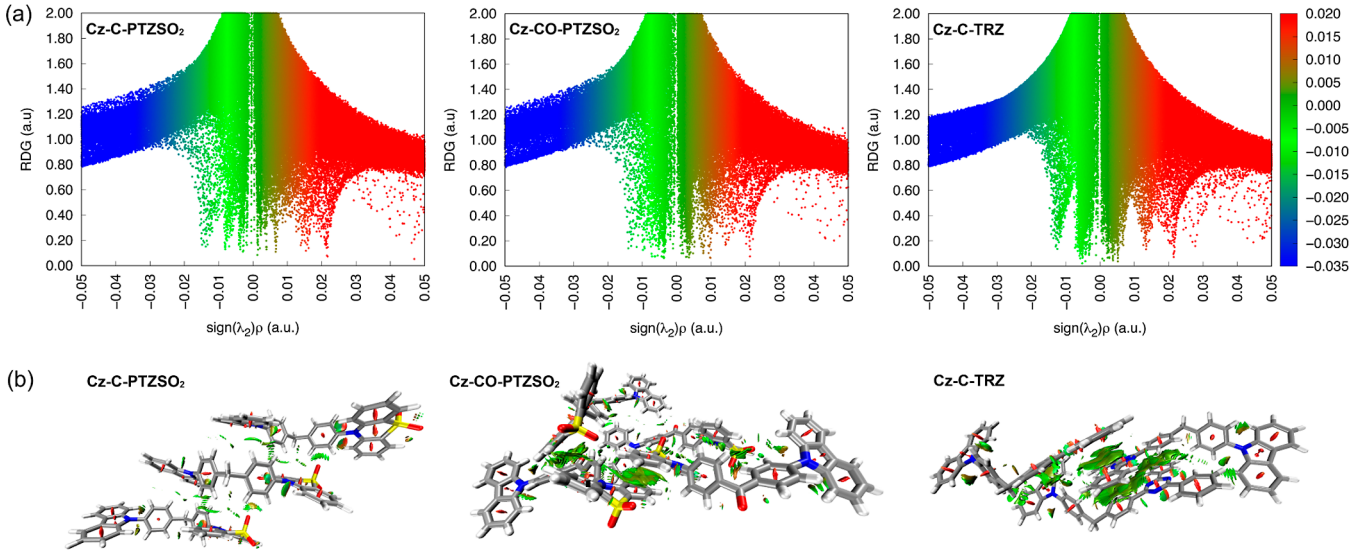

Figure 8. (a) Plots of RDG vs the electron density (ρ) multiplied by the sign of the second Hessian eigenvalue (λ_2). (b) RDG mapped with isosurfaces (isovalue: 0.6) showing intermolecular interactions.

https://doi.org/10.1021/jacs.2c12320
J. Am. Chem. Soc. XXXX, XXX, XXX−XXX

pounds, dual RTP could be enabled from both the donor and acceptor fragments due to the absence of excitonic coupling between the T_1^H and T_1^L triplet excited states. However, the excitonic coupling channel of the two states is enabled by employing an sp^2 C as a linker between the donor and acceptor moieties, resulting in only one ^{3}LE emission. Photophysical investigations substantiated this design principle. For **Cz-C-PTZSO$_2$** and **Cz-C-TRZ** crystals, dual RTP emissions from T_1^H and T_1^L states were recorded, which are LE emissions from the donor and acceptor fragments, respectively, together with the acceptor aggregate phosphorescence. For the **Cz-CO-PTZSO$_2$** crystal, only one LE T_1-dominated RTP was observed due to the strong excitonic coupling between the donor and acceptor; benefitting from the multiple intermolecular interactions, molecular aggregate phosphorescence was also activated. However, for **Cz-CO-TRZ**, there is no RTP, probably due to significant nonradiative decay. Single-crystal and RDG analyses demonstrated that noncovalent interactions influence multiple RTP behavior and TTET. This work provides insights for the design of organic systems that show dual phosphorescence and discloses an effective strategy for designing color-variable RTP that can potentially be exploited in a range of applications.

■ ASSOCIATED CONTENT

Data Availability Statement

The research data supporting this publication can be accessed at https://doi.org/10.17630/773b2b1c-dfc8-4967-be09-fbd0c8b2199e.

Supporting Information

The Supporting Information is available free of charge at https://pubs.acs.org/doi/10.1021/jacs.2c12320.

^{1}H and ^{13}C NMR spectra, HRMS, HPLC, and EA of the target compounds and supplementary computational and photophysical data (PDF)

Crystallographic data for **Cz-C-PTZSO$_2$**, **Cz-CO-PTZSO$_2$**, and **Cz-C-TRZ** (XYZ)

Accession Codes

CCDC 2203532−2203534 contain the supplementary crystallographic data for this paper. These data can be obtained free of charge via www.ccdc.cam.ac.uk/data_request/cif, or by emailing data_request@ccdc.cam.ac.uk, or by contacting The Cambridge Crystallographic Data Centre, 12 Union Road, Cambridge CB2 1EZ, UK; fax: +44 1223 336033.

■ AUTHOR INFORMATION

Corresponding Author

Eli Zysman-Colman − *Organic Semiconductor Centre, EaStCHEM School of Chemistry, University of St Andrews, Andrews KY16 9ST, U.K.;* orcid.org/0000-0001-7183-6022; Email: eli.zysman-colman@st-andrews.ac.uk

Authors

Tao Wang − *Organic Semiconductor Centre, EaStCHEM School of Chemistry, University of St Andrews, Andrews KY16 9ST, U.K.*

Abhishek Kumar Gupta − *Organic Semiconductor Centre, EaStCHEM School of Chemistry, University of St Andrews, Andrews KY16 9ST, U.K.;* orcid.org/0000-0002-0203-6256

Sen Wu − *Organic Semiconductor Centre, EaStCHEM School of Chemistry, University of St Andrews, Andrews KY16 9ST, U.K.*

Alexandra M. Z. Slawin − *Organic Semiconductor Centre, EaStCHEM School of Chemistry, University of St Andrews, Andrews KY16 9ST, U.K.;* orcid.org/0000-0002-9527-6418

Complete contact information is available at: https://pubs.acs.org/10.1021/jacs.2c12320

Notes

The authors declare no competing financial interest.

■ ACKNOWLEDGMENTS

This project has received funding from the European Union's Horizon 2020 research and innovation programme under the Marie Skłodowska Curie grant agreement no. 897098 (AIE-RTP-PLED). T.W. acknowledges support from the Marie Skłodowska-Curie Individual Fellowship. S.W. thanks the China Scholarship Council (201906250199). We thank the EPSRC (EP/R035164/1) for financial support.

■ REFERENCES

(1) Braslavsky, S. E. Glossary of Terms Used in Photochemistry, 3rd Edition (Iupac Recommendations 2006). *Pure Appl. Chem.* **2007**, *79*, 293−465.

(2) Burgert, R.; Schnöckel, H.; Grubisic, A.; Li, X.; Stokes, S. T.; Bowen, K. H.; Ganteför, G.; Kiran, B.; Jena, P. Spin Conservation Accounts for Aluminum Cluster Anion Reactivity Pattern with O2. *Science* **2008**, *319*, 438−442.

(3) Zhao, W.; He, Z.; Tang, B. Z. Room-Temperature Phosphorescence from Organic Aggregates. *Nat. Rev. Mater.* **2020**, *5*, 869−885.

(4) Hirata, S. Molecular Physics of Persistent Room Temperature Phosphorescence and Long-Lived Triplet Excitons. *Appl. Phys. Rev.* **2022**, *9*, 011304.

(5) Peng, Q.; Ma, H.; Shuai, Z. Theory of Long-Lived Room-Temperature Phosphorescence in Organic Aggregates. *Acc. Chem. Res.* **2020**, *54*, 940−949.

(6) Baryshnikov, G.; Minaev, B.; Ågren, H. Theory and Calculation of the Phosphorescence Phenomenon. *Chem. Rev.* **2017**, *117*, 6500−6537.

(7) Marian, C. M. Spin−Orbit Coupling and Intersystem Crossing in Molecules. *Wiley Interdiscip. Rev.: Comput. Mol. Sci.* **2012**, *2*, 187−203.

(8) Yan, X.; Peng, H.; Xiang, Y.; Wang, J.; Yu, L.; Tao, Y.; Li, H.; Huang, W.; Chen, R. Recent Advances on Host−Guest Material Systems toward Organic Room Temperature Phosphorescence. *Small* **2022**, *18*, 2104073.

(9) Ma, X.; Wang, J.; Tian, H. Assembling-Induced Emission: An Efficient Approach for Amorphous Metal-Free Organic Emitting Materials with Room-Temperature Phosphorescence. *Acc. Chem. Res.* **2019**, *52*, 738−748.

(10) Wu, T.; Huang, J.; Yan, Y. From Aggregation-Induced Emission to Organic Room Temperature Phosphorescence through Suppression of Molecular Vibration. *Cell Rep. Phys. Sci.* **2022**, *3*, 100771.

(11) Gu, L.; Shi, H.; Bian, L.; Gu, M.; Ling, K.; Wang, X.; Ma, H.; Cai, S.; Ning, W.; Fu, L.; et al. Colour-Tunable Ultra-Long Organic Phosphorescence of a Single-Component Molecular Crystal. *Nat. Photonics* **2019**, *13*, 406−411.

(12) Zhou, C.; Zhang, S.; Gao, Y.; Liu, H.; Shan, T.; Liang, X.; Yang, B.; Ma, Y. Ternary Emission of Fluorescence and Dual Phosphorescence at Room Temperature: A Single-Molecule White Light Emitter Based on Pure Organic Aza-Aromatic Material. *Adv. Funct. Mater.* **2018**, *28*, 1802407.

(13) Shimizu, M.; Shigitani, R.; Nakatani, M.; Kuwabara, K.; Miyake, Y.; Tajima, K.; Sakai, H.; Hasobe, T. Siloxy Group-Induced Highly Efficient Room Temperature Phosphorescence with Long Lifetime. *J. Phys. Chem. C* **2016**, *120*, 11631−11639.

(14) Yuan, W. Z.; Shen, X. Y.; Zhao, H.; Lam, J. W.; Tang, L.; Lu, P.; Wang, C.; Liu, Y.; Wang, Z.; Zheng, Q.; Sun, J. Z.; Ma, Y.; Tang, B. Z.

Crystallization-Induced Phosphorescence of Pure Organic Luminogens at Room Temperature. *J. Phys. Chem. C* **2010**, *114*, 6090−6099.
(15) Tao, Y.; Chen, R.; Li, H.; Yuan, J.; Wan, Y.; Jiang, H.; Chen, C.; Si, Y.; Zheng, C.; Yang, B.; et al. Resonance-Activated Spin-Flipping for Efficient Organic Ultralong Room-Temperature Phosphorescence. *Adv. Mater.* **2018**, *30*, 1803856.
(16) Tao, Y.; Liu, C.; Xiang, Y.; Wang, Z.; Xue, X.; Li, P.; Li, H.; Xie, G.; Huang, W.; Chen, R. Resonance-Induced Stimuli-Responsive Capacity Modulation of Organic Ultralong Room Temperature Phosphorescence. *J. Am. Chem. Soc.* **2022**, *144*, 6946−6953.
(17) Alam, P.; Cheung, T. S.; Leung, N. L. C.; Zhang, J.; Guo, J.; Du, L.; Kwok, R. T. K.; Lam, J. W. Y.; Zeng, Z.; Phillips, D. L.; et al. Organic Long-Persistent Luminescence from a Single-Component Aggregate. *J. Am. Chem. Soc.* **2022**, *144*, 3050−3062.
(18) Wang, Y.; Yang, J.; Fang, M.; Gong, Y.; Ren, J.; Tu, L.; Tang, B. Z.; Li, Z. New Phenothiazine Derivatives That Exhibit Photoinduced Room-Temperature Phosphorescence. *Adv. Funct. Mater.* **2021**, *31*, 2101719.
(19) Ren, J.; Wang, Y.; Tian, Y.; Liu, Z.; Xiao, X.; Yang, J.; Fang, M.; Li, Z. Force-Induced Turn-on Persistent Room-Temperature Phosphorescence in Purely Organic Luminogen. *Angew. Chem., Int. Ed.* **2021**, *60*, 12335−12340.
(20) Wang, T.; De, J.; Wu, S.; Gupta, A. K.; Zysman-Colman, E. Thermally Activated and Aggregation-Regulated Excitonic Coupling Enable Emissive High-Lying Triplet Excitons. *Angew. Chem., Int. Ed.* **2022**, *61*, No. e20220668.
(21) Lower, S.; El-Sayed, M. The Triplet State and Molecular Electronic Processes in Organic Molecules. *Chem. Rev.* **1966**, *66*, 199−241.
(22) Wu, Z.; Nitsch, J.; Schuster, J.; Friedrich, A.; Edkins, K.; Loebnitz, M.; Dinkelbach, F.; Stepanenko, V.; Würthner, F.; Marian, C. M.; et al. Persistent Room Temperature Phosphorescence from Triarylboranes: A Combined Experimental and Theoretical Study. *Angew. Chem., Int. Ed.* **2020**, *59*, 17137−17144.
(23) Bolton, O.; Lee, K.; Kim, H.-J.; Lin, K. Y.; Kim, J. Activating Efficient Phosphorescence from Purely Organic Materials by Crystal Design. *Nat. Chem.* **2011**, *3*, 205−210.
(24) Hamzehpoor, E.; Perepichka, D. F. Crystal Engineering of Room Temperature Phosphorescence in Organic Solids. *Angew. Chem., Int. Ed.* **2020**, *59*, 9977−9981.
(25) Yang, J.; Zhen, X.; Wang, B.; Gao, X.; Ren, Z.; Wang, J.; Xie, Y.; Li, J.; Peng, Q.; Pu, K.; et al. The Influence of the Molecular Packing on the Room Temperature Phosphorescence of Purely Organic Luminogens. *Nat. Commun.* **2018**, *9*, 840.
(26) Lee, D.; Bolton, O.; Kim, B. C.; Youk, J. H.; Takayama, S.; Kim, J. Room Temperature Phosphorescence of Metal-Free Organic Materials in Amorphous Polymer Matrices. *J. Am. Chem. Soc.* **2013**, *135*, 6325−6329.
(27) Chen, X.; Xu, C.; Wang, T.; Zhou, C.; Du, J.; Wang, Z.; Xu, H.; Xie, T.; Bi, G.; Jiang, J.; Zhang, X.; Demas, J. N.; Trindle, C. O.; Luo, Y.; Zhang, G. Versatile Room-Temperature-Phosphorescent Materials Prepared from N-Substituted Naphthalimides: Emission Enhancement and Chemical Conjugation. *Angew. Chem., Int. Ed.* **2016**, *55*, 9872−9876.
(28) Zhang, T.; Wu, Y.; Ma, X. Tunable Multicolor Room-Temperature Phosphorescence Including White-Light Emission from Amorphous Copolymers. *Chem. Eng. J.* **2021**, *412*, 128689.
(29) Louis, M.; Thomas, H.; Gmelch, M.; Haft, A.; Fries, F.; Reineke, S. Blue-Light-Absorbing Thin Films Showing Ultralong Room-Temperature Phosphorescence. *Adv. Mater.* **2019**, *31*, 1807887.
(30) Nie, X.; Su, H.; Wang, T.; Miao, H.; Chen, B.; Zhang, G. Aromatic Electrophilic Directing for Fluorescence and Room-Temperature Phosphorescence Modulation. *J. Phys. Chem. Lett.* **2021**, *12*, 3099−3105.
(31) Ding, B.; Ma, L.; Huang, Z.; Ma, X.; Tian, H. Engendering Persistent Organic Room Temperature Phosphorescence by Trace Ingredient Incorporation. *Sci. Adv.* **2021**, *7*, No. eabf9668.
(32) Zhang, Y.; Chen, X.; Xu, J.; Zhang, Q.; Gao, L.; Wang, Z.; Qu, L.; Wang, K.; Li, Y.; Cai, Z.; et al. Cross-Linked Polyphosphazene Nanospheres Boosting Long-Lived Organic Room-Temperature Phosphorescence. *J. Am. Chem. Soc.* **2022**, *144*, 6107−6117.
(33) Dai, W.; Niu, X.; Wu, X.; Ren, Y.; Zhang, Y.; Li, G.; Su, H.; Lei, Y.; Xiao, J.; Shi, J.; et al. Halogen Bonding: A New Platform for Achieving Multi-Stimuli-Responsive Persistent Phosphorescence. *Angew. Chem., Int. Ed.* **2022**, *61*, No. e202200236.
(34) Chen, C.; Chi, Z.; Chong, K. C.; Batsanov, A. S.; Yang, Z.; Mao, Z.; Yang, Z.; Liu, B. Carbazole Isomers Induce Ultralong Organic Phosphorescence. *Nat. Mater.* **2021**, *20*, 175−180.
(35) Fateminia, S. M. A.; Mao, Z.; Xu, S.; Yang, Z.; Chi, Z.; Liu, B. Organic Nanocrystals with Bright Red Persistent Room-Temperature Phosphorescence for Biological Applications. *Angew. Chem., Int. Ed.* **2017**, *56*, 12160−12164.
(36) Zhang, G.; Palmer, G. M.; Dewhirst, M. W.; Fraser, C. L. A Dual-Emissive-Materials Design Concept Enables Tumour Hypoxia Imaging. *Nat. Mater.* **2009**, *8*, 747−751.
(37) Yu, H.-J.; Zhou, Q.; Dai, X.; Shen, F.-F.; Zhang, Y.-M.; Xu, X.; Liu, Y. Photooxidation-Driven Purely Organic Room-Temperature Phosphorescent Lysosome-Targeted Imaging. *J. Am. Chem. Soc.* **2021**, *143*, 13887−13894.
(38) Wang, T.; Su, X.; Zhang, X.; Nie, X.; Huang, L.; Zhang, X.; Sun, X.; Luo, Y.; Zhang, G. Aggregation-Induced Dual-Phosphorescence from Organic Molecules for Nondoped Light-Emitting Diodes. *Adv. Mater.* **2019**, *31*, 1904273.
(39) Liu, X.; Yang, L.; Li, X.; Zhao, L.; Wang, S.; Lu, Z. H.; Ding, J.; Wang, L. An Electroactive Pure Organic Room-Temperature Phosphorescence Polymer Based on a Donor-Oxygen-Acceptor Geometry. *Angew. Chem., Int. Ed.* **2021**, *60*, 2455−2463.
(40) Wang, J.; Liang, J.; Xu, Y.; Liang, B.; Wei, J.; Li, C.; Mu, X.; Ye, K.; Wang, Y. Purely Organic Phosphorescence Emitter-Based Efficient Electroluminescence Devices. *J. Phys. Chem. Lett.* **2019**, *10*, 5983−5988.
(41) Yu, Z.; Wu, Y.; Xiao, L.; Chen, J.; Liao, Q.; Yao, J.; Fu, H. Organic Phosphorescence Nanowire Lasers. *J. Am. Chem. Soc.* **2017**, *139*, 6376−6381.
(42) Ye, W.; Ma, H.; Shi, H.; Wang, H.; Lv, A.; Bian, L.; Zhang, M.; Ma, C.; Ling, K.; Gu, M.; Mao, Y.; Yao, X.; Gao, C.; Shen, K.; Jia, W.; Zhi, J.; Cai, S.; Song, Z.; Li, J.; Zhang, Y.; Lu, S.; Liu, K.; Dong, C.; Wang, Q.; Zhou, Y.; Yao, W.; Zhang, Y.; Zhang, H.; Zhang, Z.; Hang, X.; An, Z.; Liu, X.; Huang, W. Confining Isolated Chromophores for Highly Efficient Blue Phosphorescence. *Nat. Mater.* **2021**, *20*, 1539−1544.
(43) Kasha, M. Characterization of Electronic Transitions in Complex Molecules. *Discuss. Faraday Soc.* **1950**, *9*, 14−19.
(44) Bai, D.-R.; Liu, X.-Y.; Wang, S. Charge-Transfer Emission Involving Three-Coordinate Organoboron: V-Shape Versus U-Shape and Impact of the Spacer on Dual Emission and Fluorescent Sensing. *Chem.—Eur. J.* **2007**, *13*, 5713−5723.
(45) Hudson, Z. M.; Zhao, S.-B.; Wang, R.-Y.; Wang, S. Switchable Ambient-Temperature Singlet−Triplet Dual Emission in Nonconjugated Donor−Acceptor Triarylboron−Ptii Complexes. *Chem.—Eur. J.* **2009**, *15*, 6131−6137.
(46) He, Z.; Zhao, W.; Lam, J. W. Y.; Peng, Q.; Ma, H.; Liang, G.; Shuai, Z.; Tang, B. Z. White Light Emission from a Single Organic Molecule with Dual Phosphorescence at Room Temperature. *Nat. Commun.* **2017**, *8*, 416.
(47) Wu, Y. H.; Xiao, H.; Chen, B.; Weiss, R. G.; Chen, Y. Z.; Tung, C. H.; Wu, L. Z. Multiple-State Emissions from Neat, Single-Component Molecular Solids: Suppression of Kasha's Rule. *Angew. Chem., Int. Ed.* **2020**, *59*, 10173−10178.
(48) She, P.; Duan, J.; Lu, J.; Qin, Y.; Li, F.; Liu, C.; Liu, S.; Ma, Y.; Zhao, Q. Single-Component Molecular Dual Persistent Room Temperature Phosphorescence from Low- and High-Lying Triplet States. *Adv. Opt. Mater.* **2022**, *10*, 2102706.
(49) Li, F.; Guo, S.; Qin, Y.; Shi, Y.; Han, M.; An, Z.; Liu, S.; Zhao, Q.; Huang, W. Achieving Dual Persistent Room-Temperature Phosphorescence from Polycyclic Luminophores Via Inter-/Intramolecular Charge Transfer. *Adv. Opt. Mater.* **2019**, *7*, 1900511.

https://doi.org/10.1021/jacs.2c12320
J. Am. Chem. Soc. XXXX, XXX, XXX−XXX

(50) Wang, T.; Hu, Z.; Nie, X.; Huang, L.; Hui, M.; Sun, X.; Zhang, G. Thermochromic Aggregation-Induced Dual Phosphorescence Via Temperature-Dependent Sp3-Linked Donor-Acceptor Electronic Coupling. *Nat. Commun.* **2021**, *12*, 1364.
(51) Adamo, C.; Barone, V. Toward Reliable Density Functional Methods without Adjustable Parameters: The Pbe0 Model. *J. Chem. Phys.* **1999**, *110*, 6158−6170.
(52) Petersson, G. A.; Tensfeldt, T. G., Jr.; Montgomery, J. A. A Complete Basis Set Model Chemistry. Iii. The Complete Basis Set-Quadratic Configuration Interaction Family of Methods. *J. Chem. Phys.* **1991**, *94*, 6091−6101.
(53) Lu, T.; Chen, F. Multiwfn: A Multifunctional Wavefunction Analyzer. *J. Comput. Chem.* **2012**, *33*, 580−592.
(54) Klán, P.; Wirz, J. *Photochemistry of Organic Compounds: From Concepts to Practice*; John Wiley & Sons, 2009.
(55) Connelly, N. G.; Geiger, W. E. Chemical Redox Agents for Organometallic Chemistry. *Chem. Rev.* **1996**, *96*, 877−910.
(56) Cardona, C. M.; Li, W.; Kaifer, A. E.; Stockdale, D.; Bazan, G. C. Electrochemical Considerations for Determining Absolute Frontier Orbital Energy Levels of Conjugated Polymers for Solar Cell Applications. *Adv. Mater.* **2011**, *23*, 2367−2371.
(57) Tu, D.; Cai, S.; Fernandez, C.; Ma, H.; Wang, X.; Wang, H.; Ma, C.; Yan, H.; Lu, C.; An, Z. Boron-Cluster-Enhanced Ultralong Organic Phosphorescence. *Angew. Chem., Int. Ed.* **2019**, *58*, 9129−9133.
(58) Johnson, E. R.; Keinan, S.; Mori-Sánchez, P.; Contreras-García, J.; Cohen, A. J.; Yang, W. Revealing Noncovalent Interactions. *J. Am. Chem. Soc.* **2010**, *132*, 6498−6506.

https://doi.org/10.1021/jacs.2c12320
J. Am. Chem. Soc. XXXX, XXX, XXX−XXX